Materials Today • Volume xxx, Number xx • xxxx 2020 RESEARCH

ELSEVIER

Polymer architecture as key to unprecedented high-resolution 3D-printing performance: The case of biodegradable hexa-functional telechelic urethane-based poly-ε-caprolactone

RESEARCH: Original Research

Aysu Arslan [1,†], Wolfgang Steiger [2,3,†], Patrice Roose [4], Hugues Van den Bergen [4], Peter Gruber [2,3], Elise Zerobin [3,5], Franziska Gantner [2,3], Olivier Guillaume [2,3], Aleksandr Ovsianikov [2,3,*], Sandra Van Vlierberghe [1,6,‡], Peter Dubruel [1,‡]

[1] Polymer Chemistry & Biomaterials Research Group, Centre of Macromolecular Chemistry (CMaC), Ghent University, Krijgslaan 281 S4-Bis, 9000 Ghent, Belgium
[2] 3D Printing and Biofabrication Group, Institute of Materials Science and Technology, TU Wien, 1060 Vienna, Austria
[3] Austrian Cluster for Tissue Regeneration (http://www.tissue-regeneration.at), Austria
[4] Allnex Belgium SA/NV, Anderlechtstraat 33, Drogenbos, Belgium
[5] Institute of Applied Synthetic Chemistry, TU Wien, 1060 Vienna, Austria
[6] Brussels Photonics, Department of Applied Physics and Photonics, Vrije Universiteit Brussel, Pleinlaan 2, 1050 Elsene, Belgium

Two-photon polymerization (2PP) is a high-resolution 3D-printing technology with a very rapidly expanding field of applications, including tissue engineering (TE). In this field, 2PP offers unprecedented possibilities for systematic studies of both cell–cell and cell–material interactions in 3D. For TE applications, the reliable production of biodegradable micro-scaffolds in porous, complex architectures is essential. However, the number of biodegradable materials that support the required level of spatial resolution is very limited, being a major bottleneck for the use of 2PP in the TE field.

Herein, we introduce a hexa-functional urethane-based biodegradable precursor that overcomes the limitations associated with the high-resolution printing of current biodegradable precursors. The precursor is a telechelic urethane-based poly-ε-caprolactone (PCL) possessing three acrylate functionalities at each polymer end group which enables the reliable production of complex architectures owing to its superior physical properties as compared to the traditional di-acrylate terminated analogs. The newly developed hexa-functional telechelic urethane-based PCL reveals enhanced crosslinking kinetics and one order of magnitude higher Young's modulus compared to the di-functional precursor (57.8 versus 6.3 MPa), providing an efficient and solvent-free 2PP processing at fast scanning speeds of up to 100 mm s^{-1} with unprecedented feature resolutions (143 ± 18 nm at 100 mm s^{-1} scanning speed). The crosslinked hexa-functional polymer combines strength and flexibility owing to the segregation between its hard polyacrylate and soft PCL segments, which makes it suitable for biological systems in contrast to the highly crosslinked and rigid structures typically manufactured by 2PP. Furthermore, it revealed lower degradation rate compared to its di-functional analog, which can be considered as an

* Corresponding author.
E-mail address: Ovsianikov, A. (Aleksandr.Ovsianikov@tuwien.ac.at)
† Equally contributed first authors.
‡ Equally contributed last authors.

Please cite this article in press as: A. Arslan et al., Materials Today (2020), https://doi.org/10.1016/j.mattod.2020.10.005

Nomenclature

2PP	two-photon polymerization
ε	tensile strain
σ	tensile stress
Đ	polydispersity index
ΔH°	molar reaction enthalpy of acrylate double bonds
ΔH	total reaction enthalpy
AM	additive manufacturing
C_{acr}	acrylate concentration
CAD	computer-aided design
CAM	computer-aided manufacturing
DMSO	dimethyl sulfoxide
DPC	differential photocalorimetry
EPPETA	ethoxylated and propoxylated pentaerythritol triacrylate
FTIR	Fourier transform infrared
G	storage modulus
G′	loss modulus
h_{max}	maximum heat flow
IPDI	isophorone diisocyanate
M_n	number average molar mass
M_w	weight average molar mass
NMR	nuclear magnetic resonance
n_{acr}	theoretical acrylate number
OEOacr	oligoethyleneoxide monoacrylate
P_f	final fractional acrylate conversion
PCL	poly-ε-caprolactone
R_{max}	maximum polymerization rate
SLA	stereolithography
TE	tissue engineering
T_g	glass transition temperature
U_T	deformation energy
UPCL-2	di-acrylate end-capped urethane-based poly-ε-caprolactone
UPCL-6	hexa-acrylate end-capped urethane-based poly-ε-caprolactone
UVA	ultraviolet (315 < k < 400 nm)

advantage in terms of biocompatibility due to the slower formation of acidic degradation products. Extracts of the developed polymers did not show a cytotoxic effect on the L929 fibroblasts as confirmed via ISO 10993-5 standard protocol. The presented precursor design constitutes a simple and effective approach that can be easily translated towards other biodegradable polymers for the manufacturing of biodegradable constructs with nano-scale precision, offering for the first time to use the true capabilities of 2PP for TE applications with the use of synthetic biodegradable polymers.

Introduction

Two-photon polymerization (2PP) [1], sometimes also referred to as multiphoton lithography, is a nano- and microfabrication technology with a rapidly growing field of explored applications ranging from the manufacturing of microlenses [2,3], photonic crystals [4,5], to micromechanical and microfluidic devices [6–8]. It also shows great promise as a tool to produce microscaffolds used for biomedical applications such as tissue engineering (TE) [9,10].

Its main advantage compared to available additive manufacturing (AM) methods is the capability to produce complex three-dimensional (3D) structures at a resolution of a few hundred nanometers [11]. This is achieved via two-photon absorption, a nonlinear process, which allows the highly localized deposition of light into a photosensitive resin. The absorbed light causes the creation of radicals which initiate a radical chain polymerization, leading to a densely crosslinked network. Furthermore, there is no need to add material in a layer-by-layer fashion, which is typically the case in conventional AM-technologies [1].

The exceptional resolution has rendered 2PP of interest for biomedical and TE applications. Studies reported that the cell behavior was strongly influenced by the 3D-topology of the microscaffolds produced by 2PP, indicating the importance of reliable reproduction of the structures that closely mimic the cellular microenvironment [12-14]. Here, the choice of the photosensitive resin plays a pivotal role to achieve maximal 3D-resolution through 2PP structuring. Preferably, the resin should have low optical absorption in the near-infrared region, a sufficient amount of crosslinkable groups along with fast crosslinking kinetics in order to enable the fabrication of microstructures with high resolution, along with good chemical and physical stability [15]. Low molar mass photo-crosslinkable compounds and their blends with inorganic additives are commonly used for the fabrication of microstructures with good thermal and mechanical stability [16]. These compounds form highly brittle structures upon curing and control over their final properties (physical strength, biodegradation) is limited [17]. However, for certain applications such as medical devices, drug delivery systems and TE scaffolds, the use of biocompatible materials with tunable physical characteristics is crucial [15,18].

In this respect, linear aliphatic polyesters that have been widely investigated in the biomedical field owing to their biocompatibility, degradability and tunable mechanical properties, might open up novel possibilities [19]. Poly-ε-caprolactone (PCL), is one of the most commonly used aliphatic biodegradable polyesters due to its straightforward and low-cost production routes, the tailorable physical properties and the straightforward processability [20]. It has been widely applied for the production of functional structures for a variety of biomedical applications including TE, drug delivery and wound dressings [21]. By incorporation of photo-crosslinkable functionalities (e.g. acrylates, methacrylates, etc.) via chemical modification, it can be applied in laser-based 3D-printing systems including 2PP for the production of biodegradable 3D-microscaffolds [18].

Although PCL reveals excellent potential in the biomedical field, several problems are associated with 2PP structuring of

Please cite this article in press as: A. Arslan et al., Materials Today (2020), https://doi.org/10.1016/j.mattod.2020.10.005

macromolecular precursors. These problems include the low density of crosslinkable groups, the solvent requirement, the swelling behavior and the inadequate photo-crosslinking kinetics. Consequently, the current generation materials require low writing speeds and are prone to low spatial-resolution or post-processing deformations [22,23]. The latter becomes a significant problem particularly for the production of open geometries with small feature sizes [24]. However, in the field of TE, reliable manufacturing of highly porous scaffolds with complex architectures is essential. Increasing the mechanical strength of the crosslinked networks is an effective way to decrease the post-processing deformations in 2PP [25], which can be achieved by increasing the crosslinking density. One of the well-known methods to modify the crosslink density of the networks is to alter the prepolymer molar mass [26]. Decreasing the molar mass between the crosslinking points increases the crosslinking density and thus the mechanical strength [27]. The downside of this approach includes the brittle character of the obtained networks, which is problematic for most TE applications.

To date, only a limited number of biodegradable polymers have been investigated for 2PP fabrication of microscaffolds [28–33]. Claeyssens et al. fabricated porous 3D-structures with 4 μm resolution using a biodegradable methacrylate end-capped tri-block co-polymer [28]. They reported a moderate level of distortion in the porous scaffolds as a result of shrinkage and the soft character of the material although the structure retained its shape and porosity. Pashneh-Tala et al. fabricated 3D scaffolds with minimum feature size of 10 μm using methacrylated poly (glycerol sebacate) [34]. They reported deformations or structure collapse depending on the feature size of the scaffold due to the softness of the elastomer. To date, the highest resolution reported by Melissinaki et al. was 800 nm for a methacrylated 4-arm star polylactic acid (PLA) [31]. Although the printed scaffolds retained their porous structure, bended features were visible in structures having open geometries (e.g. guidewires). In the other studies, the feature sizes of the constructs printed using biodegradable polyesters were in the order of micrometers, while the highest achievable resolutions were not mentioned. In most studies, the applied writing speeds were low (ranging between 0.05–5 mm s^{-1}). The limitation in scanning speed was imposed by the reactivity of the available material. Recently, works have demonstrated remarkable scanning speeds for 2PP applications up to 1000 mm s^{-1} [35]. However, faithful reproduction of complex architectures is still a challenging task when using synthetic biodegradable polymers [24,36]. The design and subsequent development of novel more performing materials is thus required to enable production of biodegradable structures revealing nano-scale precision.

While the synthetic biodegradable polymers that have been employed in 2PP were mainly based on di-functional linear polyesters or multi-functional star-shaped polyesters, no reports have been found covering the development of multi-functional telechelic polymers (i.e. linear polymers having more than one crosslinkable functionality on each terminus) for high-resolution 3D-printing purposes. To explore the potential of this technology, we propose herein a straightforward synthesis route for the development of a hexa-functional telechelic urethane-based PCL possessing three acrylate moieties on each terminal group. A di-functional urethane-based PCL having an identical backbone will be used as a reference material. We anticipated that the 2PP potential will be improved as a result of achieving a higher crosslinking density and an enhanced physical strength. The crosslinking kinetics, the physical strength, the solvent uptake capacity and the degradation potential of the hexa-functional telechelic precursors will be evaluated and compared to the di-functional reference counterpart. Next, the cytocompatibility of the crosslinked hexa-functional telechelic precursors will be evaluated according to the ISO 10993-5 testing protocol. In the last part of our paper, the 2PP potential of the developed precursors will be investigated.

Materials and methods

Synthesis and characterization of acrylate end-capped urethane-based PCLs

Hexaacrylate end-capped urethane-based PCL (UPCL-6) was synthesized via a 2-step modification of PCL diol (2000 g mol^{-1}, Sigma Aldrich). In a first step, molten PCL diol was reacted with isophorone diisocyanate (IPDI, Sigma Aldrich) at 75 °C for 2 h in a 1:2 stoichiometric ratio using butylated hydroxy toluene (BHT, Innochem GMBH) as radical scavenger in the presence of 300 ppm bismuth neodecanoate (Shepherd) as catalyst. In a second step, two equivalents of ethoxylated and propoxylated pentaerythritol triacrylate (EPPETA, allnex) was added to function as end-capping agent to react at 80 °C for 24 h using 300 ppm bismuth neodecanoate as catalyst. The diacrylate end-capped urethane-based PCL (UPCL-2) was synthesized according to the same protocol using a different type of end-capping agent in the second step of the reaction, which was monoacrylated oligoethyleneoxide (OEOacr, Bisomer PEA6, GEO Specialty Chemicals). The reactions were proceeded until no absorption band was observed at 2260 cm^{-1} using Fourier Transform Infrared Spectroscopy (FTIR, Perkin Elmer) indicating that the NCO groups of IPDI had completely reacted. The synthesized products were used without further purification. Chemical structures of the final products were analyzed via Fourier transform infrared (FTIR) and nuclear magnetic resonance (^{1}H NMR) spectroscopy. The data are provided in the supplementary information.

The number average molar mass (M_n), the weight average molar mass (M_w) and the polydispersity (Đ) were determined by conventional gel permeation chromatography (GPC) using polyethylene glycol (PEG) standards (Agilent Technologies, weight average molar mass range: 420–200,000 g mol^{-1}). The polymer precursors were dissolved (10 mg mL^{-1}) in chloroform (Biosolve, analytical grade) and filtered through a membrane with a 0.45 μm pore size. The analyses were performed by liquid chromatography (Alliance Waters 2695 separation module with Waters 2414 Refractive Index Detector) equipped with PLGel Mixed-D polystyrene divinylbenzene GPC columns (particle size 5 μm). The sample components were separated by the GPC columns based on their molecular size in solution and detected by a refractive index detector.

Photo-induced crosslinking of the precursors

Differential photocalorimetry (DPC)

DPC thermograms were recorded using a Mettler DSC823e equipped with a Hamamatsu Lightningcure™ LC8 lamp

Please cite this article in press as: A. Arslan et al., Materials Today (2020), https://doi.org/10.1016/j.mattod.2020.10.005

(medium-pressure mercury-xenon lamp, intensity adjusted to 15 mW cm^{-2} at 365 nm). The precursors were formulated with Irgacure 2959 (BASF) as photoinitiator (2 mol% with respect to the acrylate concentration). All measurements were conducted at 60 °C using dry nitrogen as inert flow gas (50 mL min^{-1}). Prior to irradiation, the sample was held in the molten state at 60 °C for at least 10 min using the flow of nitrogen gas to remove all dissolved oxygen. The duration of the subsequent UV-exposure step was four min. With empty crucibles the heat flow signal generated by the incident light was largely cancelled upon simultaneous illumination of the reference and sample side of the cell. However, imperfect compensation still led to a shift of the baseline upon exposure to the light source. After suitable baseline correction, the heat flow signal was scaled by the total heat of polymerization calculated from the double bond content to obtain the conversion rate. At any time, the double bond conversion p was determined by partial integration of the reaction exotherm and scaling with respect to the total heat of polymerization. The maximum polymerization rate R_{max} and final acrylate conversion p_f of the precursors were determined using Eqs. (1) and (2);

$$R_{max} = h_{max}/(C_{acr}\Delta H^o) \quad (1)$$

$$p_f = \Delta H/(C_{acr}\Delta H^o) \quad (2)$$

where h_{max} is the maximum heat flow, C_{acr} is the acrylate concentration of the precursors determined via ^{1}H NMR spectroscopy (Table 1), ΔH is the total reaction enthalpy and ΔH^o is the molar reaction enthalpy of acrylate double bonds (79 ± 1 kJ mol^{-1}) [37].

Photo-rheology

Crosslinking of the precursors upon exposure to light was also monitored using small-strain oscillatory rheology on an Anton Paar Physica MCR 300 rheometer equipped with an EXFO Novacure 2000 UVA light for sample irradiation from the bottom through a quartz plate. A parallel plate setup was used with a top plate diameter of 15 mm. In order to monitor the network formation, the storage moduli (G') and loss moduli (G'') of the solvent-free molten precursors (in presence of 2 mol% Irgacure 2959) were recorded over time upon UV exposure (15 mW cm^{-2}) at 20 °C and 60 °C. Initially, the gap between the two plates was set at 300 μm and the normal force was kept at 1 N after UV exposure. Storage and loss moduli of the materials were recorded before, during and after UV exposure for duration of 10 min, 30 min and 5 min in respective order.

Characterization of UV-crosslinked samples

Sample preparation

Thin films were prepared following a melt-casting method. As described earlier, the precursors were formulated with Irgacure 2959 as PI (2 mol% with respect to the acrylate concentration). Next, the precursors were heated to 60 °C, placed between two glass plates separated with 1 mm silicone spacer and subsequently exposed to UVA light (15 mW cm^{-2}) for 30 min. For the characterizations, triplicate samples were punched out from the thin films into the desired shape using hollow punchers as described in the upcoming sections.

Determination of tensile properties

The tensile properties were determined at room temperature using a universal testing machine (Tinius Olsen) equipped with a 500 N load cell. The crosslinked thin films were cut into dog-bone shaped samples with 1 mm thickness, 30 mm gage length and 4 mm width. A preload force of 0.3 N was applied and the specimens were tested at a cross-head velocity of 10 mm min^{-1}. Young's moduli were calculated from the initial slope of the stress–strain plots. The toughness of the materials was estimated by calculating the deformation energy (U_T) from the area under the stress–strain curve [38]:

$$U_T = \int_0^{\varepsilon_b} \sigma d\varepsilon \quad (3)$$

where σ is the tensile stress, ε is the tensile strain, ε_b is the tensile strain at break and U_T is the deformation energy.

For benchmarking, the UV-crosslinked pure EPPETA end-capping agent was also tested using the same conditions.

Determination of the loss factors

The loss factors (tanδ) of the crosslinked networks of UPCL-2, UPCL-6 and EPPETA end-capping agent were determined via dynamic mechanical measurements using an Anton Paar MCR300 rheometer with parallel-plate geometry. The samples were initially heated up to 80 °C and cooled down at a controlled rate of 3 °C min^{-1}. Loss factors of the samples were plotted as a function of temperature as an indication for the glass transition temperatures.

Determination of the solvent uptake ratio and gel fraction

The crosslinked samples were cut into disks (D: 4 mm, thickness: 1 mm) and weighed (W_i). The samples were soaked in tetrahydrofuran (THF, Sigma-Aldrich) for 24 h at room temperature and weighed in the swollen state (m_s). Next, the samples were removed, vacuum dried and weighed again (m_f). The solvent

TABLE 1

Characteristics of the developed urethane-based PCLs.

Precursor	n_{acr}	C_{acr}(mmol g^{-1})	M_n (g mol^{-1})	M_w (g mol^{-1})	Đ	R_{max}(s^{-1})	p_f
UPCL-2	2	0.60	9020	12,600	1.40	0.143	0.99
UPCL-6	6	1.74	11,300	17,400	1.54	0.246	0.95

n_{acr}: theoretical number of acrylates double bonds per molecule.
C_{acr}: concentration of double bonds determined via ^{1}H NMR analysis.
M_n: number average molar mass, M_w: weight average molar mass, Đ: polydispersity index determined via GPC analysis.
R_{max}: maximum polymerization rate and p_f: final fractional double bond conversion determined via DPC analysis.

Please cite this article in press as: A. Arslan et al., Materials Today (2020), https://doi.org/10.1016/j.mattod.2020.10.005

uptake ratios and gel fractions were determined using Eqs. (4) and (5), respectively.

$$Solvent\ uptake\ ratio = (m_s - m_f)/m_f \quad (4)$$

$$Gel\ Fraction = m_f/m_i \quad (5)$$

Determination of degradation rates via accelerated degradation study

For the accelerated degradation study, the crosslinked samples (*D*: 6 mm, thickness: 1 mm) were soaked in 5 M NaOH (37 °C) and followed gravimetrically to determine the mass loss as a result of degradation. To this end, samples were removed periodically from the degradation medium, washed with deionized water, vacuum dried and weighed using an analytical balance. For benchmarking purpose, a commercial linear PCL (M_n:10,000 g mol^{-1}, Sigma) was tested under the same conditions. The mass loss was calculated via Eq. (6);

$$Mass\ loss(\%) = \frac{m_i - m_t}{m_i} x100\% \quad (6)$$

where, m_i and m_t are the masses of the dry samples initially and after degradation, respectively.

Cytocompatibility assays

Evaluation of cytotoxicity of the crosslinked polymers

The cytocompatibility of the crosslinked hexa-functional urethane-based PCLs was tested via extraction tests in accordance with the ISO 10993-5 standard protocol with the aim to determine whether or not cytotoxic compounds are released from the samples into the media.

For sample preparation, the UPCL-6 prepolymer and Irgacure 2959 as photoinitiator (2 mol% with respect to acrylate concentration) were dissolved in THF, poured into a glass mold and dried for 2 h at 60 °C. Next, the prepolymers were crosslinked upon UV irradiation (10 J, 368 nm, UV Chamber Boekel Scientific UV Crosslinker) and the crosslinked samples were immersed in THF for an additional 3 h and dried prior to the tests.

The extract tests were conducted by immersing crosslinked UPCL-6 disks (weight: 25 mg, surface area: 3 cm^2 mL^{-1}) in high glucose Dulbecco's modified Eagle medium (HG-DMEM, Gibco, United Kingdom) supplemented with 10% NCBS and 1% penicillin–streptomycin as well as in pure dimethyl sulfoxide (DMSO) at 37 °C for 4 days (Extract-1) and 7 days (Extract-2). In parallel, extracts were prepared using melt-casted samples of commercial PCL (14,000 g mol^{-1}, Sigma) according to the same protocol. Next, the extracts were collected and used as feeding media for L929 fibroblasts. To this end, the extracts performed in cell culture medium were directly used as feeding medium for the cells (Medium A), while the pure DMSO extraction media were further diluted to 0.5% in the culture medium (Medium B) prior to application as feeding media.

The L929 fibroblasts were seeded at a density of 9.4 × 10^3 cells cm^{-2} in 96-well plates and cultivated until reaching approximately 70% confluency. Next, the culture medium was removed and the cells were incubated in 100 μL of Extract-1 for 24 h and further incubated in Extract-2 for 48 h. Extract-free Medium A and Medium B were applied as feeding medium for the cells as positive controls whereas culture medium supplemented with 10% DMSO was applied as feeding medium for the cells as negative control.

The metabolic activity of the L929 fibroblasts was assessed using PrestoBlue™ Cell Viability Reagent (Invitrogen, Fisher Scientific, Vienna, Austria) at 24 and 72 h of the culture. The fluorescence of the medium was recorded (λ_{ex} = 560 nm; λ_{em} = 590 nm) using a plate reader (Synergy™ H1 BioTeK™ plate reader, Bad Friedrichshall, Germany). The fluorescence value obtained for the cells cultivated in extract-free Medium A and Medium B was considered as 100% viability for each time point. The fluorescence values of the sample extracts were normalized against the corresponding control group and expressed relative to these 100% viabilities.

Evaluation of cytotoxicity of the catalyst

Initially, the catalyst was dissolved in DMSO at a concentration of 100 mg mL^{-1} and subsequently diluted in medium and sterile filtered to obtain a catalyst concentration of 0.1 mg mL^{-1}. Next, serial dilutions of a factor 2 was conducted in medium down to 0.0015 mg mL^{-1}.

The L929 fibroblasts were seeded at a density of 9.4 × 10^3 cells cm^{-2} in 96-well plates and cultivated until reaching approximately 70% confluency. Next, the culture medium was removed and replaced with 100 μL of catalyst dilutions (n = 6) in culture medium at seven different concentrations (0.0015–0.1 mg mL^{-1}). Then, the metabolic activity of the L929 monolayer was assessed using PrestoBlue™ Cell Viability Reagent and the metabolic activities were assessed using a plate reader as described above. The fluorescence value obtained for the cells cultivated in catalyst-free medium was considered as 100% viability. Next, all fluorescence values were normalized against this control and expressed relative to this 100% viability.

Two photon polymerization structuring

A tunable femtosecond oscillator with a repetition rate of 80 MHz (MaiTai eHP DeepSee, Spectra-Physics) was operated at 800 nm, with a pulse duration of 70 fs after the microscope objective (Plan-Apochromat 63x/1.4 Oil, Zeiss, Oberkochen, Germany). To ensure high-resolution printing, the sample was positioned using a motorized microscope stage. The laser scanning was done via a two-axis galvanometric scanner.

The solid precursors were dissolved in THF and mixed with the PI solution. 4-4′-Bis (N,N-diethylamino) benzophenone (Merck KGaA, Darmstadt, Germany) and M2CMK [39] were used as PIs. M2CMK is particularly attractive since it has a 2PA cross-section of over 100 GM units at 800 nm (1 GM = 10^{-50} cm^4 s photon^{-1}) [39]. A 10 mM stock solution of PI in THF was used in order to add PI to the resin in final concentrations of 1 wt %. The material was pipetted onto a glass slide, which was placed on a heating plate set to 60 °C for 2 h to evaporate the solvent. Before the start of the 2PP experiments, the sample was heated for 10 min at 60° C above melting temperature to increase transparency of the crystalline material, favorable for processing. For oil immersion structuring, Immersol 518 F (Zeiss, refractive index of 1.518) was used. The refractive index was measured to be 1.51. The processed samples were developed in THF for 30 min and afterwards developed in THF for an additional 10 min to remove remaining resin.

Please cite this article in press as: A. Arslan et al., Materials Today (2020), https://doi.org/10.1016/j.mattod.2020.10.005

The processing window was established by producing arrays of $50 \times 50 \times 50\ \mu m^3$ cubes at constant scanning speed of 100 mm s^{-1} [35] with increasing average laser power. Linespacing was set to 0.2 μm and the layer height was 0.5 μm for all geometries. To evaluate the resolution of the material, free-hanging lines were written in the 15 μm gap between two pillars, which were produced before the single line (Fig. 5a). This was performed at four scanning speeds (0.1, 1.0, 10, 100 mm s^{-1}), while the average laser power was increased from 2 to 100 mW in 2 mW steps (corresponding to 0.3–15 TW cm^{-2} in steps of 0.3 TW cm^{-2}). Every setting was repeated in triplicates.

Due to the fine nature of the lines, the evaporating solvent can cause capillary forces leading to rupture of fine features such as single lines. For these structures, THF was washed away using hexamethyldisilazan. This was done to submerge the fine structures in a liquid having a lower surface tension and therefore smaller capillary forces during evaporation [40]. The width of the lines were measured using scanning electron microscopy (SEM).

The reduced Young's modulus of the cubes fabricated from UPCL-6 was measured using nanoindentation. Eight cubes of $200 \times 200 \times 70\ \mu m^3$ were produced using the 20×/0.8 (Zeiss, Oberkochen, Germany) objective in this case, due to its larger field of view and therefore higher throughput. A standard three-sided Berkovich tip was used to deflect the microcantilever to record the displacement and the corresponding load. Multiple positions over the top surface of the cubes were measured. A force of 0.02 mN was selected as limit [41,42].

Results and discussion

In the present work, two different telechelic photo-crosslinkable polymers were synthesized both based on an identical poly-ε-caprolactone (PCL) backbone and urethane groups albeit terminated with a different number of crosslinkable groups. The polymers, UPCL-2 and UPCL-6, consist of respectively 2 and 6 acrylate groups on average (Fig. 1). Chemical structures of the newly developed polymers were analyzed via FTIR and proton nuclear magnetic resonance (^{1}H NMR) spectroscopy (Supplementary Information S1, S2 and S3). The acrylate concentrations of the precursors were quantified via ^{1}H NMR spectroscopy. UPCL-6 revealed a nearly three times higher acrylate concentration compared to UPCL-2 (1.74 mmol g^{-1} versus 0.60 mmol g^{-1}) as anticipated for the applied synthetic route (Table 1).

A slightly higher molar mass was observed for UPCL-6 (11,300 g mol^{-1}) compared to UPCL-2 (9020 g mol^{-1}), while both of them had an at least 3 times higher molar mass compared to the starting product PCLdiol. The latter effect can be explained by the repetition of "PCL-IPDI" units during the synthesis of the precursors due to the lower selectivity of the bismuth neodecanoate catalyst for secondary isocyanates as compared to organo-tin catalysts [43]. In addition, small fractions of low molar mass by-products were visible in the GPC

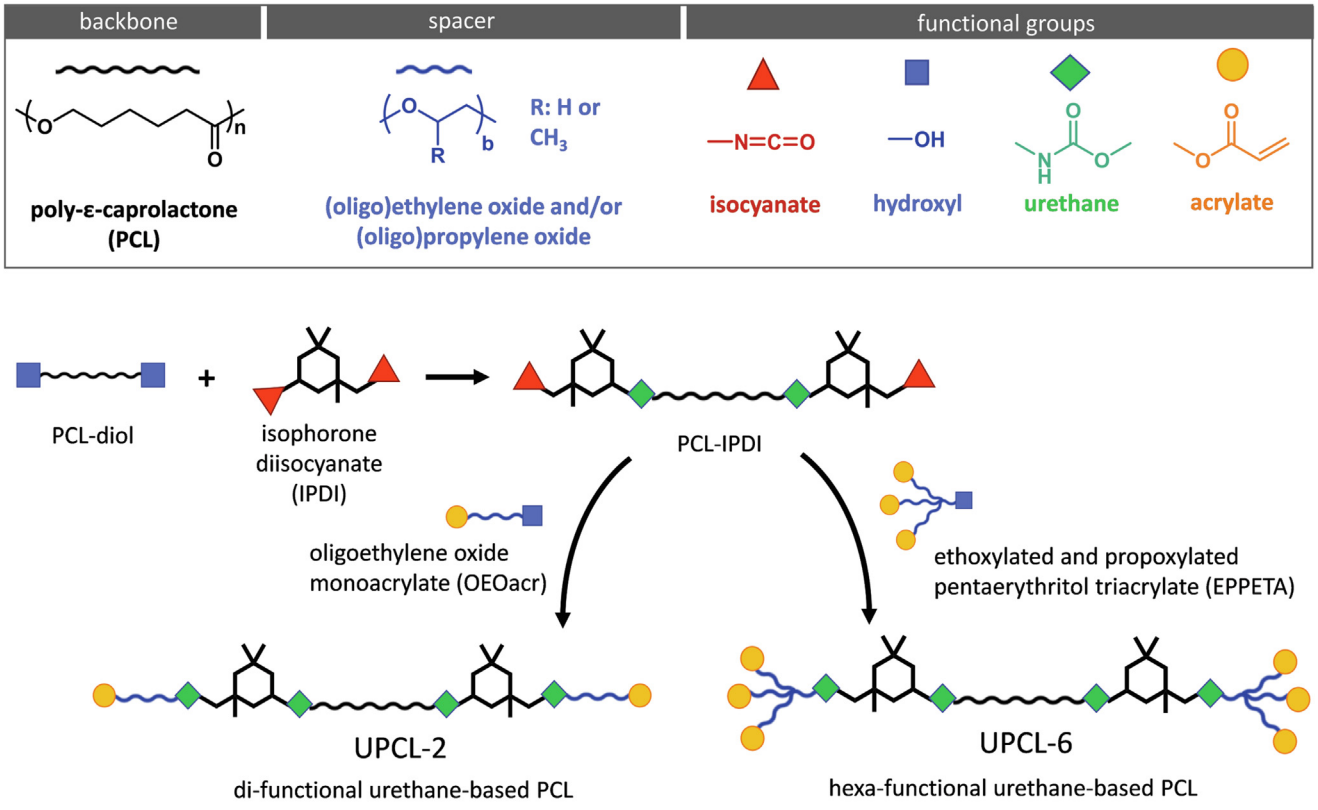

FIGURE 1

Schematic representation of the reaction steps and idealized structures of the final products UPCL-2 and UPCL-6: The two polymers were synthesized via a two-step urethanization reaction. The final products UPCL-2 and UPCL-6 are based on an identical PCL backbone albeit containing a different number of crosslinkable groups.

Please cite this article in press as: A. Arslan et al., Materials Today (2020), https://doi.org/10.1016/j.mattod.2020.10.005

chromatograms of UPCL-2 and UPCL-6, which correspond with the unreacted end-capping agents and/or the adducts formed by the reaction of IPDI with the end-capping agents. A more detailed explanation on the molar mass determination can be found in Supplementary Information S4.

Evaluation of the photo-crosslinking kinetics

The photo-crosslinking characteristics of the resins represent important criteria from the perspective of lithography-based 3D-printing systems, as the resins should ideally achieve substantial conversion in short polymerization times [18]. Although it is well-known that acrylate-based resins have a high intrinsic reactivity, other important factors such as the number of functional groups, the temperature, the photoinitiator type and concentration control the overall polymerization rate [37].

The polymerization rate vs. conversion and the conversion vs. time plots were determined based on the heat flow data obtained from DPC analysis (Fig. 2a and b). When the precursors were exposed to UV light, an immediate onset of autoacceleration was observed (Fig. 2a), which is characteristic for acrylate-based crosslinking systems [44]. Along with the transient effect to steady-state, this behavior is also attributed to a decrease in the termination constant at the early stages of reaction, as the diffusion of the terminating radicals rapidly decreases due to the growing size and restricted mobility of the radical-bearing chains [37,45]. As a result, a fast increase of the conversion was observed for both precursors in the initial stage of the crosslinking process (Fig. 2a and b).

A higher maximum polymerization rate (R_{max}) (Table 1) and a steeper increment observed for the conversion of UPCL-6 (Fig. 2b) are indications for a faster curing, which is beneficial for laser-based 3D-printing systems. At the end of the curing process, both precursors achieved a nearly complete acrylate conversion (i.e. 0.99 for UPCL-2 versus 0.95 for UPCL-6).

To date, the crosslinking characteristics of multi-functional precursors have only been investigated for monomers or oligomers with a low molar mass (e.g. pentaerythritol tetraacrylate, trimethylolpropane triacrylate, dipentaerythritol pentaacrylate, etc.) [46,47]. It has been reported by several authors that an increased number of acrylate functionalities present in the monomers or oligomers results in a decrease of the double bond conversion due to the vitrification of the highly crosslinked network and the concomitant restricted mobility of the remaining acrylates [47–50]. On the other hand, the presence of flexible

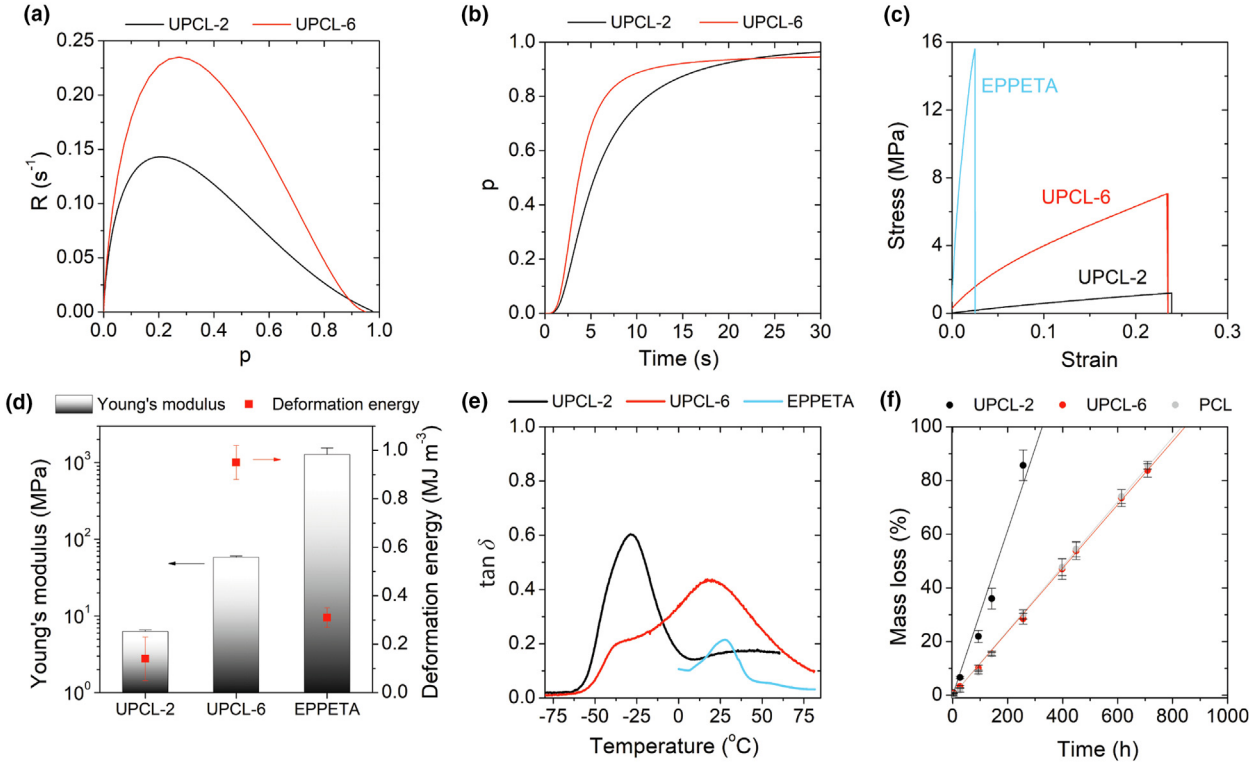

FIGURE 2

Characteristics of the precursors during and after UV-crosslinking: (a) Polymerization rate plotted as a function of fractional acrylate conversion and (b) fractional acrylate conversion as a function of time during UV-irradiation as determined via DPC analysis. The steeper increase in the polymerization rate and acrylate conversion of UPCL-6 is indicative for a higher crosslinking rate compared to UPCL-2. (c) Stress–strain plots of the crosslinked networks of UPCL-2, UPCL-6 and EPPETA (i.e. multi-functional end-capping agent of UPCL-6), (d) Young's moduli and deformation energies of the crosslinked networks of UPCL-2, UPCL-6 and EPPETA, (e) loss factor (tan δ) of the crosslinked networks of UPCL-2, UPCL-6 and EPPETA as a function of temperature and (f) mass loss of UPCL-2, UPCL-6 and a commercial linear PCL (10,000 g mol^{-1}) upon incubation in alkaline aqueous medium for 900 h at 37 °C. In (c–e), end-capping agent of UPCL-6 (EPPETA) was used as a reference low-molar-mass multi-acrylate precursor. UPCL-6 networks showed a higher strength compared to the UPCL-2 networks and enhanced toughness compared to both EPPETA and UPCL-2 networks (c and d) as a consequence of the phase segregated structure of UPCL-6 as confirmed via the presence of two glass transition temperatures in its network (e). UPCL-6 showed a complete degradation as a result of alkaline degradation albeit with a lower degradation rate compared to that of UPCL-2 (f).

Please cite this article in press as: A. Arslan et al., Materials Today (2020), https://doi.org/10.1016/j.mattod.2020.10.005

spacers separating the acrylate functionalities are known to facilitate the mobility of the reactive groups, thereby increasing the final conversion [51].

In our study, we did not observe a decrease in the reaction rate nor a remarkable decrease in the acrylate conversion when the average number of double bonds increased from 2 to 6. This can be explained by the presence of the flexible spacers separating the acrylate functionalities in this way facilitating the mobility of the reactive groups, thereby increasing the final conversion [51]. The fast polymerization rate of UPCL-6 is beneficial for reducing the laser dwell time while its high degree of acrylate conversion with minimal residual double bonds is ideal when targeting biological applications [18].

Evaluation of the properties of the crosslinked precursors

Distortion of microstructures observed after the developing step is one of the drawbacks often associated with 2PP manufacturing [24]. The low mechanical strength of the networks is considered as one of the main problems related to post-processing deformation while increasing the material stiffness enables the formation of microstructures with a higher stability [52,53]. This is especially critical for 2PP since this technology is capable of producing high spatial resolution structures with very fine features.

The mechanical properties of the crosslinked precursors were evaluated using photo-rheology and a universal tensile tester. Photo-rheology experiments revealed a nearly 12 times higher storage modulus for UPCL-6 compared to that of UPCL-2 in the plateau region, indicating a higher stiffness (Table 2). Furthermore, the precursors remained highly reactive even at temperatures as low as 20 °C and post-synthesis purification of the synthesized polymers did not result in a difference in the final moduli of the crosslinked networks (Supplementary Information S5). It is well known that an increasing amount of acrylate functionalities results in a more densely crosslinked network [54]. The higher initial acrylate concentration of the UPCL-6 led to the formation of networks with higher crosslinking density, resulting in an enhanced stiffness.

Improved mechanical strength of the urethane-based polymers as a result of an increased number of double bonds was also evidenced by the tensile tests (Table 2 and Fig. 2c and d). Indeed, increasing the average number of acrylates from 2 up to 6 resulted in a nearly ninefold increase in the Young's modulus and a fivefold increase in the ultimate tensile strength (Table 2) without reducing the strain at break of the networks significantly ($p > 0.05$). This resulted in an increased toughness as observed from the stress–strain plots (Fig. 2c).

The low-molar-mass multiacrylate monomers are known to form rigid and brittle networks upon UV curing as a result of the high glass transition temperature of the dense crosslinking [55]. Although these compounds are commonly used for laser-based 3D-printing (e.g. SLA and 2PP), their highly rigid structure is not suitable for most applications (e.g. TE) [56]. We tested the tensile properties of the crosslinked networks of EPPETA (i.e. the end-capping agent of UPCL-6, chemical structure is shown in Supplementary Information S1) as a reference low-molar-mass multi-acrylate compound for benchmarking against those of the newly developed polymers. As anticipated, the crosslinked networks of pure EPPETA showed a highly stiff (Young's modulus of 1.3 GPa) and brittle structure (strain at break: 3.4%) as derived from Fig. 2c. However, when EPPETA was covalently linked to the terminal groups of a urethane-based PCL backbone (i.e. UPCL-6), a lower modulus and an enhanced flexibility was observed. The good balance between the flexibility and the strength is observed when the hard character of the acrylic segments having a high T_g is compensated by the PCL chains having a low T_g [57]. Interestingly, dynamic mechanical thermal characterization of the UPCL-6 networks revealed two peaks for the loss factor ($\tan\delta$), reflecting the glass transition steps of locally enriched areas, i.e. the low T_g transition for the soft PCL segments (≈ -40 °C) and the high T_g transition for the hard polyacrylic chains (≈ 20 °C) (Fig. 2e). The evidence of two clear relaxation steps suggests that phase separation takes place upon crosslinking of UPCL-6 [58]. Conversely, a single glass transition around ≈ -40 °C was observed for the networks of UPCL-2, which is an indication of a uniform morphology without phase segregation. Besides its enhanced crosslinking density, the polymerization-induced phase separation in the UPCL-6 networks contributes to an enhanced toughness compared to the networks of UPCL-2 and EPPETA, where the stiff acrylate enriched phase results in an increased Young's modulus at room temperature and where the softer areas provide the required dissipation upon deformation to delay brittle failure [59].

The enhanced toughness observed for the UPCL-6 networks was also demonstrated by the deformation energies calculated from the area under the stress–strain curves of the crosslinked materials. The deformation energies of UPCL-2, UPCL-6 and EPPETA were 0.14, 0.95 and 0.31 MJ m^{-3} on average, respectively (Table 2 and Fig. 2d). The significantly higher ($p < 0.05$) deforma-

TABLE 2

Overview of the physical properties of UPCL-2, UPCL-6 and EPPETA.

Material	Plateau Modulus[a] (MPa)	Young's Modulus (MPa)	Ultimate Strength (MPa)	Strain at Break (%)	Deformation Energy (MJ m^{-3})	Solvent Uptake Ratio	Gel Fraction
UPCL-2	0.7	6.3 ± 0.3	1.3 ± 0.3	29 ± 10	0.14 ± 0.09	1.71 ± 0.04	0.97 ± 0.03
UPCL-6	8.3	57.8 ± 2.9	6.9 ± 0.2	23 ± 1	0.95 ± 0.07	0.65 ± 0.06	0.97 ± 0.03
EPPETA	N/A	1280 ± 270	14.6 ± 1.7	3.4 ± 1	0.31 ± 0.04	N/A	N/A

[a] Indicates moduli of the precursors that were irradiated at 60 °C.

Please cite this article in press as: A. Arslan et al., Materials Today (2020), https://doi.org/10.1016/j.mattod.2020.10.005

tion energy observed for UPCL-6 compared to its counterparts is indicative for a good resistance against mechanical failure and a higher toughness [38]. This is particularly interesting from the perspective of biological applications, making this material an excellent alternative in contrast to the highly crosslinked and rigid structures typically manufactured by the 2PP process using commercial resins.

Design of a telechelic urethane-based PCL with multi-acrylate terminal groups can thus be considered as an efficient approach for balancing the flexibility and the strength, which will result in the formation of networks with improved mechanical properties compared to the di-functional counterparts and the low molar mass multiacrylate monomers without a polymer backbone. Considering the particular features of the investigated multi-functional urethane-based PCLs, it can be assumed that these materials offer a great potential for many applications, including yet not limited to lithography-based 3D-printing systems, which require a fast curing process along with the formation of tough networks.

One of the reasons for the post-processing deformations typically observed in the 2PP process is the capillary force induced by the surface tension of the evaporating solvent during the developing stage [60]. The deformation of the microstructures can be reduced by decreasing the solvent uptake, which can be accomplished by increasing the crosslinking density [61]. Determination of the solvent uptake capacity for both precursors revealed a nearly 3-fold decrease in the solvent uptake when the average number of double bonds per molecule was increased from 2 up to 6 (Table 2) as expected from an increase in crosslink density. Gel fractions of nearly 1.0 were found for both polymers indicating effectively crosslinked networks. (Table 2).

There is a strong demand for polymers with controlled degradation properties particularly for biomedical applications such as drug delivery and TE. Aliphatic polyesters are commonly used biodegradable materials as they undergo hydrolytic degradation by random scission of ester bonds. Their degradation can be accelerated in an OH^- rich medium with an alkali-promoted hydrolysis [62,63]. Here, the degradation rates of the UPCL-2 and UPCL-6 networks were analyzed using a basic medium (5 M NaOH) and benchmarked against a commercial linear PCL (10,000 g mol^{-1}) that has a similar molar mass compared to the precursors used in this study.

The mass losses of the polymers upon alkaline degradation are shown in Fig. 2f. Crosslinked networks of UPCL-2 showed the highest rate of degradation resulting in a complete mass loss in 300 h. The time required for a complete degradation of UPCL-6 was found to be nearly 2.5 times higher than that of UPCL-2. However, the degradation rate of UPCL-6 was found to be similar to that of commercial linear PCL. The higher degradation rate observed for UPCL-2 is in agreement with previous work from Meseguer-Duenas, who observed a higher degradation rate for crosslinked di-functional PCL networks compared to a linear non-crosslinked PCL [62]. They attributed this behavior to the higher hydrophilicity and the lower crystallinity of the crosslinked, di-functional PCL, in which NaOH could diffuse into the network unlike the linear PCL having higher crystallinity. Although UPCL-6 networks do not have a crystalline structure, as evidenced via differential scanning calorimetry (Supplementary Information S6), their degradation rate was observed to be lower than that of UPCL-2 most likely as a result of the high crosslinking density and the closely packed polyacrylate chains. Nevertheless, it eventually showed complete degradation with a rate similar to linear, non-crosslinked PCL. Slower degradation of UPCL-6 can potentially be an advantage in terms of biocompatibility, as high degradation rates are associated with lower cell viabilities *in vitro* and *in vivo* due to the local acidic environment created by rapid degradation and carboxylic acid formation [64]. The typical duration for a complete degradation of PCL is reported to be several years (2–4 years depending on the molar mass) [20]. Based on the data of our accelerated tests, the complete degradation of UPCL-6 can be anticipated to be in the order of several years similar to that of commercial PCL. However, the degradation pathway (bulk vs. surface degradation) might be different in accelerated and long-term degradation, which can result in different relative degradation rates in a long-term study [63]. To have more reliable data related to the long-term degradation behavior, the results will be further confirmed via degradation tests in buffer and *in vivo*.

PCL is a biocompatible aliphatic polyester that has been approved by the Food and Drug Administration in various applications [20]. However, the chemical modification routes that are applied to obtain photopolymerizable prepolymers might induce potential adverse effects on the cell viability (e.g. leachable chemical substances). In order to determine whether or not cytotoxic compounds from the crosslinked UPCL-6 samples are released into the media, we performed cytocompatibility tests according to the ISO 10993-5 standard protocol as well as a direct cytotoxicity assay to evaluate the cytocompatibility of bismuth neodecanoate, which was used as catalyst for the synthesis of the prepolymers.

Fig. 3a depicts the relative metabolic activity of L929 fibroblasts that were cultured in the extracts of crosslinked UPCL-6 and in those of a commercial, non-modified PCL. The extractions performed in cell culture medium revealed no significant adverse effect on the viability of L929 fibroblasts up to 72 h of the culture for any of the applied materials (Medium A, $p > 0.05$ in comparison with the extract-free control group), as an indication that no cytotoxic compounds are released into the cell culture medium from UPCL-6 throughout an extraction period up to 7 days. The extractions that were conducted in DMSO revealed a significant reduction in cell viability after 24 h of the culture (Medium B, $p < 0.01$ in comparison with the extract-free control group). However, no significant difference was evident between the extracts of UPCL-6 and commercial PCL, indicating that the reduction in cell viability was not due to leachable chemical substances that are associated with the synthesis of the crosslinkable prepolymer. Nevertheless, at the end of 72 h of culture, the viability of the cells that were cultured in these extracts was comparable to that of the control group ($p > 0.05$). The morphology of the fibroblasts that were cultured in sample extracts from both media were similar to those of the positive control groups at all time points (Supplementary Information S7). Despite their well-known biocompatibility, PCL-based structures are not cell-interactive due to their synthetic and hydrophobic nature. Indeed, a moderate wettability was observed for crosslinked UPCL-6 based on static contact

Please cite this article in press as: A. Arslan et al., Materials Today (2020), https://doi.org/10.1016/j.mattod.2020.10.005

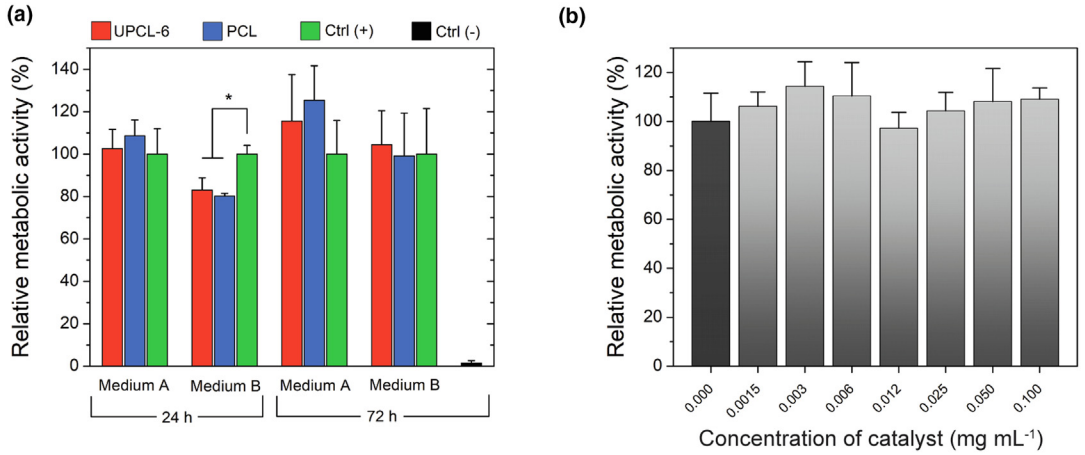

FIGURE 3

(a) Relative metabolic activity of L929 fibroblasts cultured in sample extracts or extract-free media for 24 and 72 h. (Medium A and Medium B correspond to culture medium and culture medium containing 0.5% DMSO, respectively. Ctrl (+) is extract-free Medium A or Medium B as positive control groups and Ctrl (−) is culture medium supplemented with 10% DMSO as negative control group.) No adverse effect was evidenced on the viability L929 fibroblasts associated with the synthesis of UPCL-6. (b) Relative metabolic activity of L929 fibroblasts cultured in medium supplemented with bismuth neodecanoate at seven different concentrations. No cytotoxic effect was evidenced from the catalyst at the applied concentration range. (The statistical analysis was performed by one-way ANOVA with Tukey post-test, with $*p < 0.01$, $n = 6$.)

angle measurements (Supplementary Information S9). The hydrophilicity and cell-interactivity of the PCL scaffolds can be improved substantially through various physical and chemical surface modification strategies as already reported earlier by our research group [65]. However, the evaluation of surface functionalization on the cell response was beyond the scope of the present work.

During the production of urethane-based compounds, the reaction of polyols and isocyanates are typically catalyzed by organo-tin catalysts (e.g. dibutyl tin dilaurate). Although organo-tin catalysts provide excellent properties in terms of reactivity (e.g. high reaction rate and selectivity), these compounds are highly toxic for almost any kind of cells, which restricts their use in biomedical applications. Furthermore, organo-tin catalysts are systematically being substituted by alternative catalysts due to both environmental and toxicological concerns [66,67]. Bismuth carboxylates are excellent alternatives as catalysts for the synthesis of urethane-based polymers owing to their versatility and low toxicity [66,68]. In our study, we applied Bismuth neodecanoate as catalyst for the prepolymer synthesis. Although it is known that Bismuth based compounds reveal low toxicity, a cytotoxicity study of Bismuth neodecanoate has not been reported to date.

A direct cytotoxicity assay performed on the Bismuth neodecanoate revealed no significant cytotoxic effect ($p > 0.05$, in comparison with catalyst-free culture medium) in the applied concentration range (0.0015–0.1000 mg mL^{-1}) (Fig. 3b). The non-toxic single dose of Bi-salts that can be taken by a patient has been reported earlier as 1–10 mmol [66]. Considering the concentration of catalyst used in the synthesis of UPCL-6 prepolymer (0.6 mg g^{-1} or 8.3 × 10^{-4} mmol g^{-1}), we anticipate that the scaffolds produced by the polymers in this study will not involve any risk of toxicity due to the presence of catalyst.

Overall, these tests confirmed that the newly developed polymers are cytocompatible even without performing a post-synthesis purification. This is beneficial for the use of the suggested polymer in biomedical applications while opening up upscaling opportunities without the need for expensive post-synthesis purification steps.

Evaluation of the two-photon polymerization performance

Initially, UPCL-2 was structured via 2PP using two different photoinitiators. The comparison between 1 wt % 4,4′-bis (N,N-diethylamino) benzophenone and 1 wt % M2CMK was realized by fabricating arrays of cubes with increasing average laser power. The results showed that an average energy of 40 mW was required when using 4-4′-bis (N,N-diethylamino) benzophenone whereas upon applying 1 wt % M2CMK, the threshold decreased down to 10 mW. For UPCL-6 containing 1 wt % M2CMK, a threshold as low as 5 mW was reached. The arrays of cubes printed for both precursors are included in Supplementary Information S10.

Complex geometries structured with UPCL-2 (containing 1 wt % M2CMK) were not stable after development. Free-standing geometries collapsed after evaporation of the solvent (Fig. 4 b, c). Increasing the average laser power up to 200 mW did not yield more stable structures despite the higher amount of energy deposited into the resin. In comparison, UPCL-6 processed using 100 mW and 1 wt % M2CMK yielded stable 3D-structures after development (Fig. 4d, e). Furthermore, the low water uptake capacity of crosslinked UPCL-6 (<2%, Supplementary Information S9), is advantageous with respect to incubation of these scaffolds in cell-culture medium while avoiding swelling-related deformations.

Microstructures fabricated from UPCL-2 collapsed most likely due to their low crosslinking density and concomitant low stiffness. Although the properties could be improved by increasing the number of acrylates, these compounds would reveal potentially negative effects for TE applications due to the residual acrylates. The exact acrylate conversion of UPCL-6 after the 2PP

Please cite this article in press as: A. Arslan et al., Materials Today (2020), https://doi.org/10.1016/j.mattod.2020.10.005

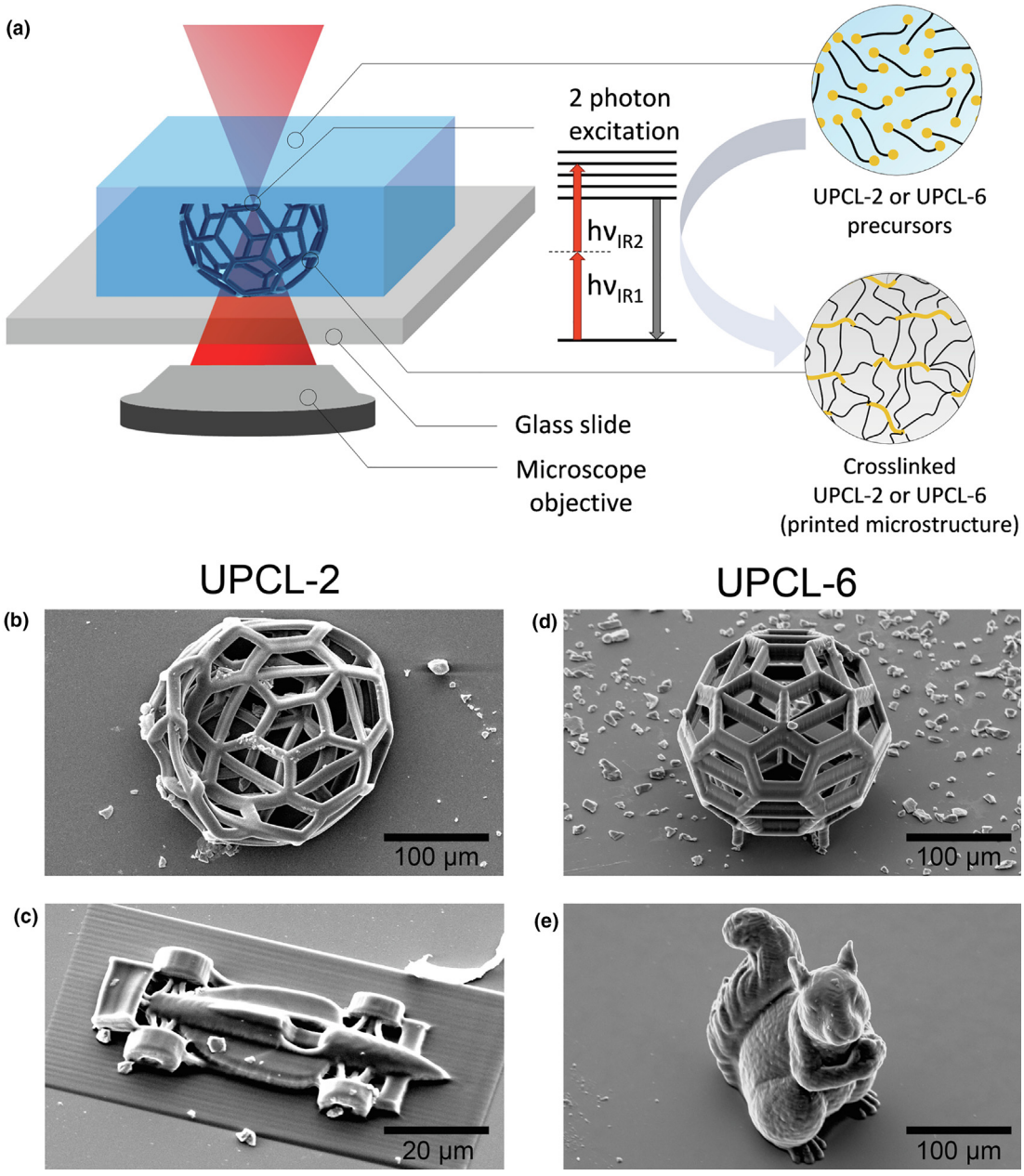

FIGURE 4

(a) Simplified representation of the 2PP process. Porous microstructures were printed via solvent-free processing of both UPCL-2 and UPCL-6 precursors individually. Simultaneous absorption of two photons in a highly localized volume enables fabrication of microstructures with resolutions down to a few hundred nanometers. (b and c) SEM images of freestanding 3D-structures based on UPCL-2 and (d and e) those of UPCL-6 fabricated in the presence of 1 wt % M2CMK. Free-standing structures from UPCL-2 collapsed after development (b and c). With UPCL-6 all geometries were stable after development (d and e). Fine microscaffolds like buckyballs from UPCL-6 (d) remained stable even after development and did not collapse as the UPCL-2 counterparts (b).

process is unknown. However, a nearly complete acrylate conversion has been observed based on the DPC experiments (Table 1), indicating the suitability of the UPCL-6 precursors for TE applications.

The resolution of UPCL-6 was evaluated by writing free-hanging lines in the 15 µm gap between two pillars (Fig. 5a), which were produced before the single line. UPCL-6 was processable at writing speeds up to 100 mm s^{-1}, while a minimum feature size below 150 nm was achieved (Table 3, Fig. 5c). The required laser power for a line at 100 mm s^{-1} was 18 mW compared to 5 mW observed when writing cubes (Supplementary Information S10). This result was anticipated as a 3D structure such as a cube consists of multiple adjacent irradiation areas. A single voxel within the cube is surrounded by similarly irradiated areas from which radicals can diffuse into the adjacent voxel and the depletion of polymerization quenchers, such as oxygen, playing a similar role [16,69].

The reduced Young's modulus of the 2PP structured UPCL-6 was found to be 39.7 ± 9.8 MPa based on nanoindentation studies, which is comparable to values obtained for commercially available 2PP-photoresists (Supplementary Information S13) [70]. Owing to the effect of the 2PP fabrication process on the

Please cite this article in press as: A. Arslan et al., Materials Today (2020), https://doi.org/10.1016/j.mattod.2020.10.005

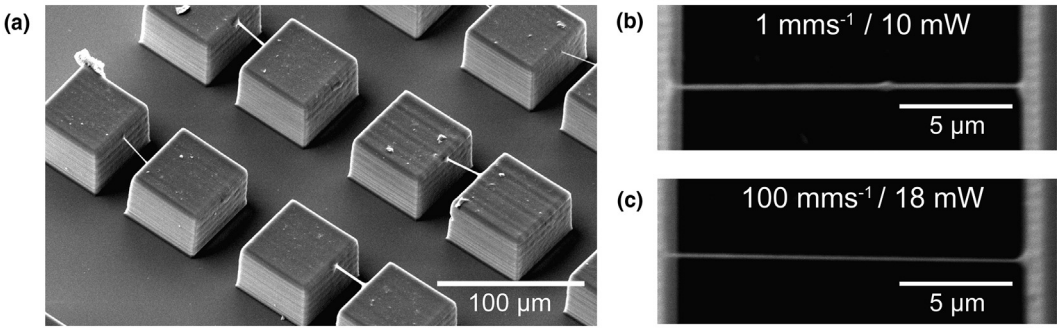

FIGURE 5

Free-hanging lines produced between two pillars using UPCL-6. The laser power was increased in steps of 2 mW, showcased in the SEM image (a) of developed structures. An intensity of 10 mW was required to obtain lines at a scanning speed of 1 mm s^{-1} with a line width of 310 ± 8 nm (b). For a writing speed of 100 mm s^{-1} an average power of 18 mW was required to yield a line width of 143 ± 18 nm (c).

TABLE 3

Minimum feature resolution extracted from free-hanging lines structured using UPCL-6 containing 1 wt % M2CMK. The minimum laser power required to observe lines after developing the sample increased with increased writing speed as the local exposure time was reduced. The highest feature resolution was <150 nm at 100 mm s^{-1}.

Writing Speed (mm s^{-1})	Laser power (mW)	Width (nm)
0.1	6	377 ± 13
1.0	10	310 ± 8
10.0	14	287 ± 59
100.0	18	143 ± 18

material properties, these values are difficult to directly compare with values reported earlier for samples fabricated with conventional AM methods. Further studies are required to determine, whether or not the mechanical properties can be significantly improved by increasing the laser power and the scanning speed [71]. This is of particular interest as PCL-based microscaffolds fabricated via selective laser sintering (SLS) have already been reported by Williams et al. as a potential material for bone and cartilage repair [72]

To the best of our knowledge, the minimum feature size (143 ± 18 nm) we achieved using the hexa-functional urethane-based PCL in our study is the highest resolution ever reported for a synthetic biodegradable polymer. To date, very few synthetic biodegradable polymers have been reported for the 2PP fabrication of microstructures. Among them, the highest resolution was reported to be 800 nm for a methacrylated 4-arm star polylactic acid (PLA) [31]. Although promising results were obtained for the 2PP structured biodegradable polymers in the TE field, their fabrication into stable complex architectures with high precision has not been reported to date. According to earlier studies, nano-patterns produced by various fabrication methods could have significant impact on cellular functions compared to micro-patterns [73–75]. For instance, differentiation of human mesenchymal stem cells was reported to be enhanced significantly on the nano-gratings of 350 nm width compared to those having 1 and 10 μm width [74]. We believe that, the resolution range achieved using the suggested polymers in this study will open up novel possibilities for guiding cell behavior on biodegradable scaffolds produced by 2PP for the first time. The process can potentially be further improved thanks to recent advancements in multiphoton absorption. For instance, the use of higher order nonlinear absorption processes (i.e. from 3 to 7-photon absorption) has been suggested to further improve spatial resolution as a result of a greater spatial confinement [76]. Furthermore, it was reported that, pentaerythritol triacrylate could be polymerized in the absence of a photoinitiator as a result of photoionization of the monomer molecules with a seventh-order nonlinear absorption [77]. The latter can be considered as an advantage for the fabrication of biomaterials while avoiding the potential toxicity of the multiphoton initiators.

One of the major practical issues related to 2PP processing is the deformation or collapse of 3D-structures, which results from the capillary forces induced by the surface tension of the evaporating developer [24,78]. The resist pattern collapse problem has been well-studied earlier for ultrafine microlithography applications [25,79–81]. It has been reported that the pattern collapse depends on the dimensions and the aspect ratio (i.e. height/width) of the printed pattern. When the aspect ratio is above a critical point, patterns tend to bend or break as a result of the capillary forces [79]. One of the methods to overcome this issue is increasing the material stiffness [81–83]. Tanaka et al. reported that the critical aspect ratio of a pattern with 0.15 μm width could be increased from 5 up to 6.7 by increasing the resist hardness [83]. Thus, the mechanical characteristics of the material play a prominent role in the deformation particularly for the geometries with large aspect ratios. These studies were however based on 2D patterning of photoresists in-plane dimensions. Although the collapse effect in 2PP cannot be simply defined by the aspect ratio due to the complexity of the 3D-geometry, one can expect that the effect of material strength will be more prominent on the stability of hollow architectures with thin features rather than bulky designs [25]. Consequently, the reliability and the stability of the printed structure becomes dependent on the feature size of the free-standing parts. For instance, Pashneh-Tala et al. reported that, an increase in the pillar thickness up to 25 μm was required in order to prevent 2PP-fabricated poly(glycerol sebacate) scaffolds against collapsing [34]. This limitation in controlling the feature sizes renders microstructuring challenging particularly for TE applications, where the generation of highly porous scaffolds with small feature sizes is essential.

Please cite this article in press as: A. Arslan et al., Materials Today (2020), https://doi.org/10.1016/j.mattod.2020.10.005

In our study, we tested the 2PP performances of two precursors using a buckyball design as a model for a considerably open geometry (Fig. 4 b and d) with a surface porosity of 65%. In contrast to the collapsed structures of UPCL-2, structures with high shape fidelity could be achieved with the stronger material UPCL-6. Although the final acrylate conversions of the developed polymers are unknown in the 2PP process, the failure of structuring UPCL-2 is not likely due to a potential incomplete crosslinking reaction, since increasing the laser power up to 200 mW did not improve the morphology of the printed structures. This is an indication that even though a high fractional acrylate conversion is achieved in the UPCL-2 networks, the concentration of its crosslinkable groups (C_{acr} = 0.60 mmol g^{-1}, Table 1) was most likely not high enough to create networks with a sufficient mechanical strength to resist the deformation. In contrast, designing a hexa-functional precursor resulted in inherently stiffer crosslinked networks as a result of an increased concentration of crosslinkable groups (1.74 mmol g^{-1}, Table 1) and phase segregation behavior (Fig. 2e), enabling the reliable production of the complex designs with the same dimensions.

Thompson et al. studied the 2PP performance of PCL diacrylate (PCLDA) and PCL triacrylate (PCLTA) and obtained promising results in terms of retinal biocompatibility [84]. They reported an improvement in 2PP performance (i.e. shape fidelity, threshold) when the total number of acrylate groups were increased from two (i.e. PCLDA) up to three (i.e. PCLTA) in the prepolymer due to the increased crosslinking density of the crosslinked networks. In their preceding study, the crosslinked PCLTAs had a lower toughness compared with that of PCLDA (53–61 kJ m^{-3} versus 90–150 kJ m^{-3}) [85], which is an indication that phase separation is lacking in PCLTA in contrast with our product UPCL-6. Interestingly, they reported a decrease in the accuracy of the 2PP process when the molar mass of PCLTA from 300 g mol^{-1} was increased up to 900 g mol^{-1}, which was attributed to a decreased concentration of the crosslinkable groups. The concentration of acrylate groups in the prepolymer PCLTA (900 g mol^{-1}) can be approximately calculated as > 2.6 mmol g^{-1} (with the assumption of a degree of acrylation 79% or higher, as reported in their preceding study [85]), being remarkably higher than that of our UPCL-6 (i.e. 1.74 mmol g^{-1}). The latter suggests that, besides the concentration of crosslinkable groups, other factors might be responsible for the accuracy of microstructuring in our study, such as the phase separation behavior associated with the polymer architecture of UPCL-6. The formation of a second glass transition at higher temperatures associated with the two-phase structure of UPCL-6 gives a remarkable rise to the stiffness of the crosslinked polymer at room temperature compared to that of di-functional counterparts (57.8 versus 6.3 MPa), which is advantageous in terms of maintaining the shape fidelity of the printed microstructures. We anticipate that, these unique advantages offered by the polymer architecture will most likely provide more freedom in formulations. For instance, even at slightly lower acrylate concentrations or higher molar masses, a good performance in high-resolution 3D printing can be anticipated. Evaluation of the lower limit for acrylate concentration, or the upper limit for prepolymer molar mass to obtain stable microstructures were beyond the scope of this work, however, will be evaluated in a future study.

In earlier studies, alternative approaches were applied to improve the biomechanical performance of PCL scaffolds printed via different rapid prototyping techniques. Gloria et al. used the blends of PCL and poly(ester amide) (PEA) for fabrication of 3D scaffolds via an extrusion-based bioprinter. They reported a significant increase in the storage and Young's moduli of the scaffolds by increasing the amount of PEA [86]. De Santis et al. developed 3D magnetic scaffolds based on a PCL matrix reinforced with iron oxide or iron-doped hydroxyapatite nanoparticles [87]. They reported an improvement in stiffness and cell behavior in PCL matrices upon incorporation of iron oxide or iron-doped hydroxyapatite into PCL matrix. In case of crosslinkable PCLs, increasing the crosslinking density is usually associated with the formation of stiffer but less flexible networks [88]. Although high stiffness is desired from the processing point of view, the use of highly brittle materials is a drawback for many applications [38]. In our study, using multiple crosslinkable end-groups without altering the backbone molar mass resulted in stiffer networks with a similar strain at break owing to the phase-segregation behavior, thus providing a trade-off between stiffness and toughness. The mechanical properties of the model precursor can be further modulated by adjusting the chemistry of their building blocks (i.e. backbone, diisocyanate type, number of crosslinkable groups), which will broaden the range of biodegradable materials available for reliable TE scaffold production. Indeed, in an earlier study of our research group, we developed a series of di-acrylate end-capped urethane-based poly (ethylene glycol) (PEG), which showed tailorable mechanical properties upon altering the molar mass of the PEG backbone [89]. More specifically, by increasing the PEG molar mass from 2000 up to 8000 g mol^{-1}, final moduli decreased from 0.6 down to 0.1 MPa. Similarly, it can be anticipated that by varying the chemistry of the backbone of hexa-functional precursors (e.g. varying the molar mass or applying a softer or stiffer biodegradable polymer), the mechanical properties of the final networks can be tuned towards different TE applications.

Earlier studies demonstrated the behavior of cells to depend on the dimensions of the substrates obtained using the 2PP technology with non-degradable materials. Jeon et al. studied the behavior of fibroblasts on anisotropic cross patterns and parallel line patterns with controlled dimensions fabricated via 2PP [90]. They reported that the cell migration speeds were enhanced by the cross patterns depending on the grid aspect ratio and the grid size. When the grid size was smaller than the size of individual cells (16 μm), the cell migration speed was significantly enhanced. Creff et al. showed that the differentiation of the Caco-2 intestinal epithelial cells was improved on 3D-scaffolds fabricated by 2PP that accurately mimic the native architecture of the intestinal epithelium [12]. These advancements indicate the great potential of 2PP technology for the fabrication of 3D-scaffolds with precisely controlled topologies, enabling systematic studies of cell behavior [9].

While TE strategies mainly constitute scaffold-based and scaffold-free approaches, recently a promising third strategy that combines both approaches was proposed [36,91]. In the new synergetic strategy, the cell spheroids are directly produced within microscaffolds, which are highly porous and facilitate the fusion of neighboring spheroids while shielding them from

Please cite this article in press as: A. Arslan et al., Materials Today (2020), https://doi.org/10.1016/j.mattod.2020.10.005

mechanical damage. Although this synergetic strategy holds great promise in the TE field by integrating the advantages of both approaches, one of the bottlenecks is still the limited availability of biodegradable materials compatible with the 2PP technology [36]. To date, the majority of the materials that were investigated for the 2PP production of scaffolds, were based on non-biodegradable materials. The proposed biodegradable precursor model in this study offers a great promise in the field of TE for both the scaffold-based and the synergetic approaches.

Future perspectives include the functionalization of the scaffold with ECM proteins [92], growth factors [93] or nanoclays [89], which will promote the cell-material interactions.

Conclusion

In the present work, the physical properties and the 2PP processing potential of newly developed multi-acrylate terminated telechelic polymer were studied for the first time, while comparing their performance with a di-functional counterpart. The hexa-functional UPCL-6 outperformed the di-functional UPCL-2 in terms of 2PP processing, as a result of its improved crosslinking kinetics, a higher strength as well as a lower solvent uptake. The molecular architecture of the hexa-functional urethane-based PCLs enabled segregation between the hard polyacrylate and the soft polymer segments, leading to an enhanced toughness as well as an enhanced stiffness which is particularly interesting from the perspective of laser-based 3D-printing systems and biological applications. Despite having multiple acrylate moieties, they achieved a nearly complete acrylate conversion owing to the flexible spacer groups linked between its acrylate groups while they are potentially degradable as confirmed from the accelerated degradation studies. The developed polymers are biocompatible even without post-synthesis purification, as evidenced from the cytocompatibility tests.

Reliable reproduction of complex 3D-scaffolds showed the processability of UPCL-6 using 2PP and renders this a potential material for scaffold-based TE applications. It could be processed into microstructures with high feature resolutions (143 ± 18 nm) and was processable at high scanning speeds (100 mm s^{-1}) even in the absence of a solvent, as required for high-throughput 2PP applications. This material represents a real breakthrough enabling the realization of biodegradable 2PP microscaffolds for the third strategy in TE, which is based on the integration of the scaffold-based and scaffold-free approaches.

With its unique characteristics, the multi-functional telechelic urethane-based PCLs emerge as attractive candidates for the 2PP production of complex architectures with excellent shape fidelity particularly for biological applications. Moreover, the production of the multi-functional telechelic polymers offers a straightforward and solvent-free "one-pot" synthesis without requiring expensive post-synthesis purification steps, which can potentially be applied on an industrial scale. This approach can easily be translated towards other polymer backbones (e.g. different biodegradable polymers or synthetic hydrogel building blocks), which will broaden the biocompatible feedstock polymers available for 2PP manufacturing of microstructures enabling fast processing as well as excellent CAD-CAM mimicry.

CRediT authorship contribution statement

Aysu Arslan: Conceptualization, Investigation, Writing - original draft. **Wolfgang Steiger:** Conceptualization, Investigation, Writing - original draft. **Patrice Roose:** Conceptualization, Resources, Writing - review & editing. **Hugues Van den Bergen:** Resources, Writing - review & editing. **Peter Gruber:** Software, Validation. **Elise Zerobin:** Resources, Writing - review & editing. **Franziska Gantner:** Validation, Investigation. **Olivier Guillaume:** Investigation. **Aleksandr Ovsianikov:** Supervision, Writing - review & editing. **Sandra Van Vlierberghe:** Supervision, Writing - review & editing. **Peter Dubruel:** Supervision, Writing - review & editing.

Declaration of Competing Interest

The authors declare that they have no known competing financial interests or personal relationships that could have appeared to influence the work reported in this paper.

Acknowledgements

Financial support by the European Research Council (Consolidator Grant 772464) and FWO-FWF grant (Research Foundation Flanders—Austrian Science Fund project, FWOAL843, #I2444N28) is gratefully acknowledged. Peter Dubruel acknowledges the Research Foundation Flanders (FWO, Belgium) for the research grant G030217N. The authors want to thank Thomas Koch (TU Wien) for nanoindentation measurements and Marica Markovic (TU Wien) for assistance in sample preparation for cell culture experiments.

Data Availability

The raw/processed data required to reproduce these findings cannot be shared at this time as the data also forms part of an ongoing study.

Appendix A. Supplementary data

Supplementary data to this article can be found online at https://doi.org/10.1016/j.mattod.2020.10.005.

References

[1] J. Stampfl, R. Liska, A. Ovsianikov, Multiphoton Lithography: Techniques, Materials, and Applications, John Wiley & Sons, 2016.
[2] S. Thiele et al., Sci. Adv. 3 (2017) e1602655.
[3] R. Guo et al., Opt. Express 14 (2006) 810–816.
[4] M. Deubel et al., Opt. Lett. 31 (2006) 805.
[5] M.D. Turner, G.E. Schröder-Turk, M. Gu, Opt. Express 19 (2011) 10001.
[6] L. Amato et al., Lab Chip 12 (2012) 1135.
[7] C. Schizas et al., Int. J. Adv. Manuf. Technol. 48 (2010) 435–441.
[8] P. Galajda, P. Ormos, J. Opt. B Quantum Semiclassical Opt. 4 (2002) S78–S81.
[9] A. Ovsianikov et al., Expert Rev. Med. Devices 9 (2012) 613–633.
[10] B. Guillotin et al., Biomaterials 31 (2010) 7250–7256.
[11] W. Haske et al., Opt. Express 15 (2007) 3426.
[12] J. Creff et al., Biomaterials 221 (2019) 119404.
[13] H. Do Cha et al., J. Micromech. Microeng. 22 (2012).
[14] T. Zandrini et al., Sci. Rep. 9 (2019) 1–9.
[15] K.T. Nguyen, J.L. West, Biomaterials 23 (2002) 4307–4314.
[16] J. Serbin, A. Ovsianikov, B. Chichkov, Opt. Express 12 (2004) 5221–5228.
[17] S. Orman et al., J. Polym. Sci. Part A Polym. Chem. 57 (2019) 110–119.
[18] A.K. Nguyen, R.J. Narayan, Mater. Today 20 (2017) 314–322.
[19] I. Manavitehrani et al., Polymers (Basel) 8 (2016) 20.
[20] M.A. Woodruff, D.W. Hutmacher, Prog. Polym. Sci. 35 (2010) 1217–1256.

Please cite this article in press as: A. Arslan et al., Materials Today (2020), https://doi.org/10.1016/j.mattod.2020.10.005

[21] Z. Muwaffak et al., Int. J. Pharm. 527 (2017) 161–170.
[22] A. Berg et al., Adv. Eng. Mater. 13 (2011) B274–B284.
[23] A. Tudor et al., Mater. Today 21 (2018) 807–816.
[24] S.-H. Park et al., Microelectron. Eng. 85 (2008) 432–439.
[25] C.C. Chang et al., Soft Matter 10 (2014) 8542–8547.
[26] F.C. Campbell, Thermoset resins: the glue that holds the strings together, in: Manufacturing Processes for Advanced Composites, Elsevier, 2004, pp. 63–101.
[27] A.N. Fraga, V.A. Alvarez, A. Vazquez, J. Compos. Mater. 37 (2003) 1553–1574.
[28] F. Claeyssens et al., Langmuir 25 (2009) 3219–3223.
[29] R.M. Felfel et al., Biomed. Mater. 11 (2016) 015011.
[30] T. Weiß et al., Adv. Eng. Mater. 13 (2011) B264–B273.
[31] V. Melissinaki et al., Biofabrication 3 (2011) 045005.
[32] P. Danilevicius et al., Appl. Surf. Sci. 336 (2015) 2–10.
[33] G. Weisgrab, et al., Biofabrication 12 (2020) 045036 (https://doi.org/10.1088/1758-5090/abb539).
[34] S. Pashneh-Tala, et al., 6, 41 (2018).
[35] A. Dobos, et al., Adv. Healthc. Mater. 0, 1900752 (n.d.).
[36] A. Ovsianikov, A. Khademhosseini, V. Mironov, Trends Biotechnol. 36 (2018) 348–357.
[37] P. Roose et al., Macromolecules 51 (2018) 5027–5038.
[38] S.C. Ligon-Auer et al., Polym. Chem. 7 (2016) 257–286.
[39] A. Ajami et al., Appl. Phys. Lett. 111 (2017) 071901.
[40] J.R. Jones et al., Biomaterials 28 (2007) 1653–1663.
[41] K. Cicha et al., J. Appl. Phys. 112 (2012) 094906.
[42] B.J. Briscoe, L. Fiori, E. Pelillo, J. Phys. D. Appl. Phys. 31 (1998) 2395–2405.
[43] R. Lomolder, F. Plogmann, P. S.-hqis Ag, J. Coat. Technol. 69, 51–57 (1997).
[44] E. Andrzejewska, Prog. Polym. Sci. 26 (2001) 605–665.
[45] M.D. Goodner, C.N. Bowman, Macromolecules 32 (1999) 6552–6559.
[46] K.S. Anseth, C.M. Wang, C.N. Bowman, Macromolecules 27 (1994) 650–655.
[47] I.V. Khudyakov et al., Ind. Eng. Chem. Res. 38 (1999) 3353–3359.
[48] M. Schuster et al., Monatsh. Chem. Chem. Mon. 138 (2007) 261–268.
[49] T.J. White, W.B. Liechty, C.A. Guymon, J. Polym. Sci. Part A Polym. Chem. 45 (2007) 4062–4073.
[50] K.S. Anseth, C.M. Wang, C.N. Bowman, Polymer (Guildf) 35 (1994) 3243–3250.
[51] W.F. Jager et al., Macromolecules 30 (1997) 780–791.
[52] J. Van Hoorick et al., Biomacromolecules 18 (2017) 3260–3272.
[53] D. Jin et al., Mater. Today 32 (2020) 19–25.
[54] I.V. Khudyakov, Prog. Org. Coatings 121 (2018) 151–159.
[55] J.S. Young, A.R. Kannurpatti, C.N. Bowman, Macromol. Chem. Phys. 199 (1998) 1043–1049.
[56] P. Dorfinger, J. Stampfl, R. Liska, Mater. Sci. Forum 825–826 (2015) 53–59.
[57] R.A. Ryntz, P.V. Yaneff, Coatings of Polymers and Plastics, CRC Press, 2003.
[58] T.A. Speckhard et al., J. Appl. Polym. Sci. 30 (1985) 647–666.
[59] M. Szycher, Szycher's Handbook of Polyurethanes, CRC Press, 1999.
[60] E. Käpylä et al., Mater. Sci. Eng. C 43 (2014) 280–289.
[61] F. Klein et al., Adv. Mater. 23 (2011) 1341–1345.
[62] J.M. Meseguer-Dueñas et al., J. Mater. Sci. Mater. Med. 22 (2011) 11–18.
[63] C.X.F. Lam et al., Biomed. Mater. 3 (2008) 034108.
[64] H.-J. Sung et al., Biomaterials 25 (2004) 5735–5742.
[65] T. Desmet et al., Macromol. Biosci. 10 (2010) 1484–1494.
[66] H.R. Kricheldorf, Chem. Rev. 109 (2009) 5579–5594.
[67] W.J. Blank, Macromol. Symp. 187 (2002) 261–270.
[68] H.R. Kricheldorf, G. Behnken, G. Schwarz, Polymer (Guildf) 46 (2005) 11219–11224.
[69] A. Pikulin, N. Bityurin, V.I. Sokolov, AIP Adv. 5 (2015) 127215.
[70] A. Doraiswamy et al., J. Nanosci. Nanotechnol. 10 (2010) 6305–6312.
[71] T. Koch, S. Seidler, Macromol. Symp. 181 (2002) 499–506.
[72] J.M. Williams et al., Biomaterials 26 (2005) 4817–4827.
[73] K.S. Brammer et al., Acta Biomater. 7 (2011) 683–690.
[74] E.K.F. Yim, S.W. Pang, K.W. Leong, Exp. Cell Res. 313 (2007) 1820–1829.
[75] C.Y. Tay et al., Small 7 (2011) 1361–1378.
[76] D.S. Corrêa et al., Opt. Commun. 277 (2007) 440–445.
[77] J. Fischer et al., Opt. Express 21 (2013) 26244.
[78] D.Y. Yang et al., Appl. Phys. Lett. 90 (2007) 2005–2008.
[79] W.-D. Domke et al., Pattern collapse in high-aspect-ratio DUV and 193-nm resists, Advances in Resist Technology and Processing XVII, 2000.
[80] T. Tanaka et al., Jpn. J. Appl. Phys. 33 (1994) L1803–L1805.
[81] H.B. Cao, P.F. Nealey, W.-D. Domke, J. Vac. Sci. Technol. B Microelectron. Nanom. Struct. 18 (2000) 3303.
[82] D.-Y. Yang et al., Appl. Phys. Lett. 90 (2007) 079903.
[83] T. Tanaka, J. Electrochem. Soc. 141 (1994) L169.
[84] J.R. Thompson et al., Acta Biomater. 94 (2019) 204–218.
[85] B.J. Green et al., Biomacromolecules 19 (2018) 3682–3692.
[86] A. Gloria et al., Mater. Sci. Eng. C 98 (2019) 994–1004.
[87] R. De Santis et al., Virtual Phys. Prototyp. 6 (2011) 189–195.
[88] C. Ma et al., Biomaterials 178 (2018) 383–400.
[89] A. Mignon et al., React. Funct. Polym. 136 (2019) 95–106.
[90] H. Jeon et al., Biomaterials 31 (2010) 4286–4295.
[91] T. Ren et al., Biofabrication 12 (2020) 025033.
[92] Y. Wang et al., Sci. Rep. 6 (2016) 37427.
[93] T.-M. De Witte et al., Regener. Biomater. 5 (2018) 197–211.

Please cite this article in press as: A. Arslan et al., Materials Today (2020), https://doi.org/10.1016/j.mattod.2020.10.005